Scaling of Dorsal-Ventral Patterning by Embryo Size-Dependent Degradation of Spemann's Organizer Signals

Hidehiko Inomata,[1,3,*] Tatsuo Shibata,[2] Tomoko Haraguchi,[1] and Yoshiki Sasai[1,*]
[1]Organogenesis and Neurogenesis Group
[2]Laboratory for Physical Biology
RIKEN Center for Developmental Biology, Kobe 650-0047, Japan
[3]Precursory Research for Embryonic Science and Technology (PRESTO) Program, Japan Science and Technology Agency, 4-1-8 Honcho, Kawaguchi, Saitama, 332-0012, Japan
*Correspondence: hideino@cdb.riken.jp (H.I.), yoshikisasai@cdb.riken.jp (Y.S.)
http://dx.doi.org/10.1016/j.cell.2013.05.004

SUMMARY

Spemann's organizer plays a key role in dorsal-ventral (DV) patterning in the amphibian embryo by secreting diffusible proteins such as Chordin, an antagonist to ventralizing bone morphogenetic proteins (BMPs). The DV patterning is so robust that an amphibian embryo with its ventral half surgically removed can develop into a smaller but proportionally patterned larva. Here, we show that this robust patterning depends on facilitated Chordin degradation and requires the expression of the Chordin-proteinase inhibitor Sizzled on the opposite side. Sizzled, which is stable and diffuses widely along the DV axis, stabilizes Chordin and expands its distribution in the ventral direction. This expanded Chordin distribution, in turn, limits BMP-dependent Sizzled production, forming an axis-wide feedback loop for shaping Chordin's activity. Using bisection assays, we demonstrate that Chordin degradation is dynamically controlled by embryo-size-coupled Sizzled accumulation. We propose a scaling model that enables the DV pattern to adjust proportionally to embryonic axis size.

INTRODUCTION

In *Xenopus*, sperm entry triggers the dorsal-ventral (DV) polarity formation, causing cortical rotation and activating canonical Wnt signaling in a dorsally predominant manner (Heasman, 2006). This Wnt activation, which depends on maternal β-catenin, induces the gene network that determines the side of Spemann's organizer after the midblastula transition (Spemann and Mangold, 1924), including genes that encode organizer-specifying transcription factors, such as Goosecoid, and secreted organizer factors (De Robertis, 2009; De Robertis and Kuroda, 2004).

In *Xenopus*, positional information along the DV axis is primarily given by local bone morphogenetic protein (BMP) signals,

which instruct ventralization. The organizer provides dorsal positional values by secreting BMP antagonists such as Chordin and Noggin (Piccolo et al., 1996; Sasai et al., 1994; Smith and Harland, 1992), which generate a reverse BMP signal gradient along the DV axis (dorsal-low/ventral-high). If the organizer factors are depleted, the whole embryo is hyperventralized because of increased activity of BMP4, which is autonomously produced from zygotic transcripts (Khokha et al., 2005). The gastrula of *Xenopus laevis* has a diameter of ∼1.1 mm, which is fairly large compared to the mammalian gastrula. Given the substantial perturbations that can affect an amphibian embryo developing in the wild, it is surprising that a single signaling center, the organizer, is able to shape a robust pattern across this relatively long distance during the short period of frog gastrulation.

Closely related amphibian species that are thought to have patterning molecules with similar properties can vary widely in embryo sizes. In fact, eggs and gastrulae of the same species (e.g., *Xenopus laevis*) occasionally differ in size; yet despite the size differences, they still give rise to embryos with indistinguishable patterns (Figures S1A–S1C available online). An even more remarkable example of the robust shape similarity in *Xenopus* is the self-regulatory phenotype after bisection (Kimelman and Pyati, 2005; Reversade and De Robertis, 2005). When a blastula embryo is physically bisected into dorsal and ventral halves, the dorsal piece, which autonomously forms the organizer, develops into a proportionally patterned smaller embryo along the DV axis—instead of having disproportionately large dorsal tissues, as would be expected from its origin. Thus, the dynamic adjustment of the axial pattern to the embryonic size, termed scaling (Ben-Zvi et al., 2011), is an important characteristic of DV patterning by the organizer, one that cannot be easily explained by simple diffusion of the same set of molecules. In our present study, we address this scaling issue by elucidating an axis-wide feedback control system for Chordin distribution, which is controlled by the secreted Chordin proteinase inhibitor Sizzled (Lee et al., 2006; Muraoka et al., 2006).

Xenopus DV patterning involves multiplex feedback mechanisms with strong resilience and robustness. For instance, even if a half of the organizer tissue is removed by resection, the embryo can develop normally by regaining proper organizer

function (Cooke, 1973, 1975). This strong autoregulatory system could partly mask phenotypic responses to signal perturbations in the dorsal domain. This robustness requires at least two key molecules, ADMP, or antidorsalizing morphogenetic protein (Reversade and De Robertis, 2005) and ONT1, an Olfactomedin-class secreted scaffold protein (Inomata et al., 2008). ADMP, a unique BMP molecule expressed in the dorsal axis, gives a ventralizing signal, and ADMP's expression is negatively regulated by BMP signaling (therefore positively by Chordin), forming a negative feedback system for limiting the organizer activity (Reversade and De Robertis, 2005).

Another layer of complexity arises from Wnt signaling, which plays opposite roles at two distinct phases (Heasman, 2006). The maternal canonical Wnt pathway produces a "prepattern" with a strong dorsal bias (Figure S1D, blue), which complicates the direct analysis of BMP-dependent DV patterning during gastrulation. In addition, after the organizer forms, the embryo's lateral-ventral domain expresses zygotic *wnt* genes such as *wnt8*, whose products exert moderate ventralizing effects on gastrula tissues (Christian and Moon, 1993; Figure S1D, green). Because midrange BMP signaling induces the expression of these zygotic *wnt* genes (Marom et al., 1999), this also makes the direct readout of BMP patterning signals more difficult by exerting indirect effects via Wnts.

In the present study, to understand the direct effect of organizer signals on the dynamic spatiotemporal modulation of the "BMP signaling field" along the DV axis, we conducted reconstitution experiments using a combination of multigene knockdown and RNA microinjection. We demonstrate that the dynamic state of Sizzled protein conveys the axis size information for scaling via controlling stability of Chordin protein.

RESULTS

Graded DV Pattern in a Reconstituted System Depends on Chordin

To remove complexities introduced by prepatterning and secondary zygotic events, we first depleted canonical Wnt signaling in the early *Xenopus* embryo by inhibiting β-catenin with antisense morpholino oligonucleotides (β-catenin-MOs) (Figure S1E), which causes radial ventralization (Figures 1A–1C). This hyperventralization depended on the enhancement of endogenous BMP signaling by the absence of the organizer-derived BMP antagonists; the embryo became radially dorsalized through additional suppression of BMP signals (Figure 1D; see radial *shh* expression) using MOs against all four major BMP ligands (4BMPs, hereinafter BMP2/4/7 and ADMP; Reversade et al., 2005; Reversade and De Robertis, 2005).

Using this homogenously ventralized embryo, we next performed a reconstitution assay (Figures 1E–1G) in which a "dorsal" axis was exogenously created by locally inhibiting BMP signaling with injecting dominant-negative BMP receptor (*dnBR*) messenger RNA (mRNA) in a single vegetal blastomere of the β-catenin-depleted eight-cell embryo (Figure S1F). The *dnBR*-expressing cells in the late gastrula (marked with a *LacZ* tracer; red in Figure 1E) expressed the axial marker *Shh*, indicating that these cells were committed to the dorsal midline

(organizer) fate. It is interesting that localized dnBR expression exerted sufficiently long-range effects to generate a whole DV pattern. For intance, the *sizzled*[+] "ventral" domain was limited to a small area on the side opposite the dnBR-expressing domain (Figure 1E), whereas large domains between the two became partially dorsalized into paraxial-lateral tissues (hereinafter referred to as lateral domains).

This non-cell-autonomous effect by *dnBR* was largely dependent on BMP antagonists emanating from the *dnBR*-induced organizer. Attenuation of Chordin by MO strongly expanded the *sizzled*[+] ventral domain and diminished the areas of the lateral domains in the reconstituted embryo with *dnBR* (Figure 1F). In contrast, the injection of *noggin*-MO, regardless of the dosage, had a marginal effect, if any (Figure 1G; data not shown). On the other hand, the effect of *chordin*-MO was enhanced by coinjection of *noggin*-MO (data not shown); therefore, it turned out that, under these reconstitution conditions, Noggin actually contributed to the DV pattern but only to an extent that could be largely compensated by Chordin under these conditions (Figure 1H).

We next compared their effects in a reconstitution assay in which we depleted endogenous Chordin and Noggin in addition to β-catenin, using MOs for all three mRNAs (*βCN*-MO) (Figure S1F). Under this triple-gene knockdown condition (which caused radial ventralization; Figures 1I–1L), we created a "dorsal" domain by injecting *chordin* or *noggin* mRNA (having comparable activation; Figure S1G) at various dosages into a single blastomere in the eight-cell embryo. This reconstitution assay allowed us to independently assess quantitatively controlled effects of *chordin* and *noggin* on the BMP signaling field without the complexities introduced by mutual induction and autoactivation (Figure S1H).

Injection of *chordin* mRNA (25–100 pg per cell) generated a graded DV pattern with distinct dorsal, lateral, and ventral domains (Figures 1M–1P, S1I, and S1J) as seen in the *dnBR*-injected embryo; this is consistent with Chordin playing a major role in the graded DV pattern. As with *chordin*, *noggin* injection also suppressed *sizzled* expression and induced *shh* and *myoD* expression. However, there was a qualitative difference in DV marker distribution (Figures S1K–S1N). At a moderate dosage (25 pg per cell), *noggin* promoted nearly radial *myoD* expression (Figure S1L). At a higher dosage (100 pg per cell), *noggin* induced rather diffuse *shh* expression that was not localized to the injection site (Figures S1M and S1N). Thus, when expressed in a localized region, *chordin* efficiently generates a graded DV pattern along the whole axis in the ventral-default embryo, whereas *noggin* tends to raise the general level of dorsal information (Figures 1P and S1N). Consistent with these observations, *noggin* injection suppressed nuclear pSmad1 accumulation (indicative of high BMP signals) in the entire *βCN* MO-injected embryo (Figure S2A–S2C), whereas *chordin* injection substantially decreased pSmad1 at the injection side but not at the opposite end (Figure S2D).

Chordin Distribution Is Limited by Proteolysis Rather Than Diffusion

Chordin activity is negatively regulated by the Tolloid-class proteinases specific to Chordin (Piccolo et al., 1997), and this
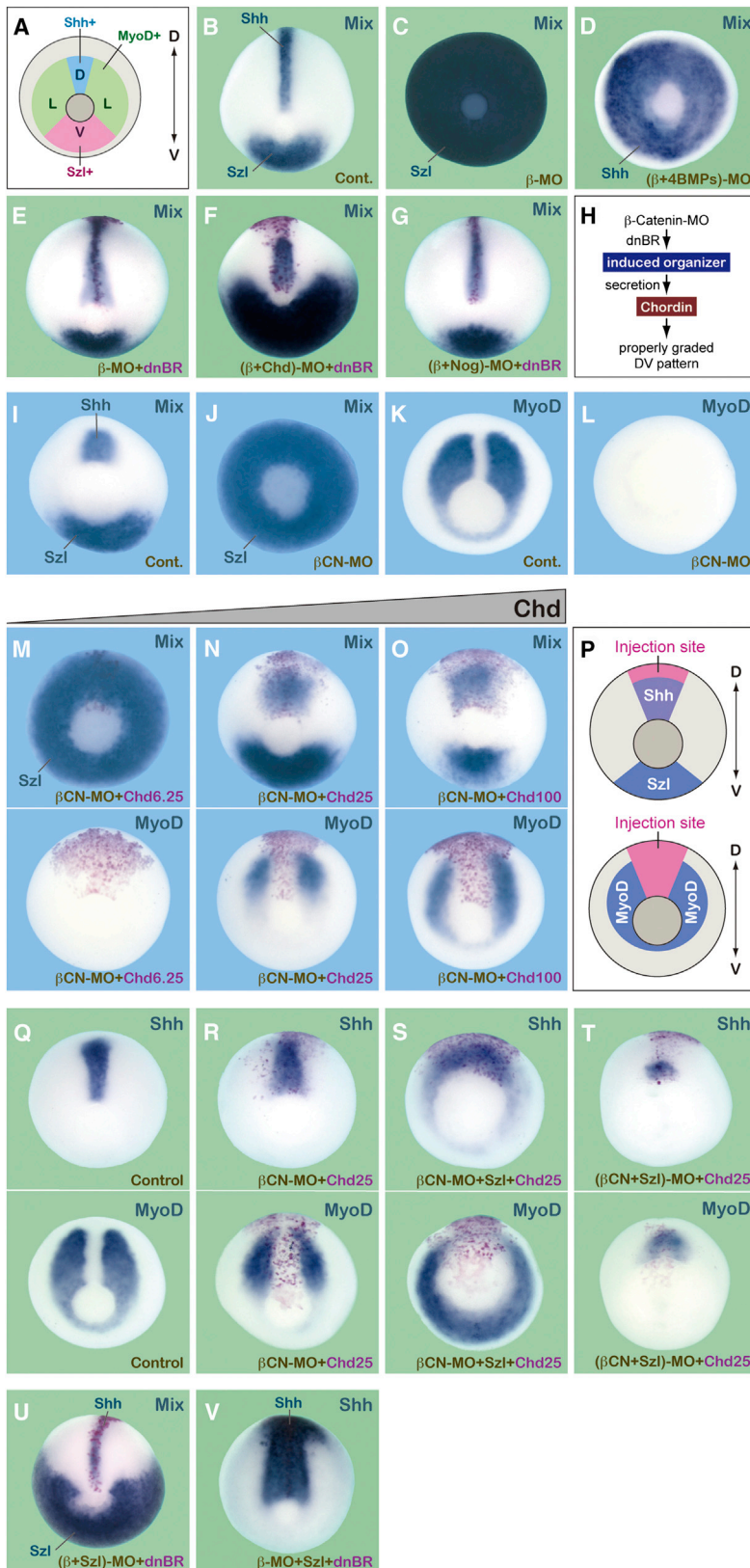
Figure 1. Graded DV Patterning by the Organizer Depends on Chordin

(A) Schematic of DV pattern in the control (Cont.) stage 12.5 embryo. D, dorsal; L, lateral; V, ventral.

(B) Whole-mount in situ hybridization with *shh* (dorsal axial) and *sizzled* (Szl) (ventral) probes (Mix probes, hereinafter).

(C) β-*catenin*-MO-injected embryo with radial expression of *sizzled* (100%, n = 20).

(D) Radial *shh* expression in the embryo injected with β-*catenin*-MO and MOs against four major *bmp* genes: *bmp4*, *admp*, *bmp2*, and *bmp7* (100%, n = 11).

(E) Single-blastomere injection of *dnBR* (shown by the *LacZ* tracer in red; 200 pg) rescued the DV pattern in the β-*catenin*-MO-injected embryo (100%, n = 13).

(F) Single-blastomere injection of *dnBR* in the embryo injected with β-*catenin*- and *chordin*-MOs. Dorsal expansion of *sizzled* expression was seen. Compare with (E); 100%, n = 15.

(G) Single-blastomere injection of *dnBR* in the embryo injected with β-*catenin*- and *noggin*-MOs. No *sizzled* expansion (87.5%, n = 16).

(H) Summary of (E)–(G).

(I–T) Reconstitution experiments using the triple-knockdown embryo with MOs for β-*catenin*, *chordin* (Chd), and *noggin*. (I) through (L) show marker expression in the triple-knockdown embryo at stage 12 (J) *sizzled* and (L) *myoD*; (I) and (K) show controls. (M–O) Single-blastomere injection of *chordin* (the *LacZ* tracer in red) rescued the DV pattern in the triple-knockdown embryo; 100%, n = 12, for (N) and 85.7%, n = 14, for (O), judged by mixed probes. In (M), at a smaller dosage (6.25 pg), no dorsal-lateral region was observed. (P) Schematic of results in (M) through (O). (Q) through (T) show the effects of overexpression (S) and depletion (T) of *sizzled* on DV markers in the triple-knockdown embryo rescued by *chordin* (R) (25 pg); control is shown in (Q). (S) Substantial expansion of *shh* and *myoD* (86.7%, n = 15 and 100%, n = 16) by *sizzled* mRNA injection at the two-cell stage (400 pg). (T) Substantial reduction of *shh* and *myoD* (100%, n = 17 and n = 16) by *sizzled*-MO injection at the two-cell stage.

(U and V) Effects of loss (U) and gain (V) of Sizzled's function on the DV pattern. (U) shows substantial expansion of *sizzled* (100%, n = 20), and (V) shows substantial expansion of *shh* (87%, n = 23).

See also Figures S1 and S2.

Chordin-specific degradation is inhibited by a secreted protein-ase inhibitor encoded by *sizzled* (Lee et al., 2006; Muraoka et al., 2006). In a reconstitution assay in the *βCN*-MO embryo, the over-expression or depletion of Sizzled augmented or attenuated dorsalizing effects of exogenously delivered *chordin* along the DV axis, respectively (Figures 1Q–1T). Notably, when Chordin degradation was inhibited by Sizzled overexpression (Figure 1S), the *myoD*[+] domain widely expanded to the ventral end, as seen in the embryo dorsalized by local *noggin* expression (Figure S1L). Consistent with these findings, long-range suppressing effects of *chordin* on pSmad1 accumulation (Figure S2D) were augmented and inhibited by gain and loss, respectively, of Siz-zled's function (Figures S2E–S2J). In addition, Sizzled-mediated control of Chordin degradation had a strong impact on the non-cell-autonomous patterning activity of *dnBR*-induced organizer tissue in the β-catenin-depleted embryo (compare Figures 1U and 1V with Figure 1E). When Sizzled was inhibited in the *β-catenin* MO embryo rescued with *dnBR*, the ventral marker strongly expanded dorsalward (Figure 1U), consistent with the Chordin-depletion phenotype (Figure 1F).

In our reconstitution assay, Chordin production is exoge-nously controlled independently of secondary transcriptional events (Figure S1H). Therefore, these findings explicitly demon-strated that facilitated degradation of Chordin plays a major role in its effect on graded DV patterning. We next investigated the molecular aspect of this regulation at the protein level (Figure 2). In particular, we asked whether Chordin's ability to generate the graded DV pattern is related to its property of degradation or diffusion, two critical factors for the extent of the molecule's spreading.

Unlike Chordin, there are no specific proteinases known to facilitate proteolysis of Noggin. To directly examine protein sta-bility in vivo, we microinjected recombinant *Xenopus* Chordin and Noggin proteins (26.7 fmol per embryo, each) into the blas-tocoel of the late blastula (Inomata et al., 2008; Reversade and De Robertis, 2005) (Figures 2A–2D). Chordin disappeared from the embryo promptly after being injected (Figure 2B, row 1), with a half-life of ∼30 min (Figure 2C). The rapid degradation of Chordin was dependent on Chordin proteinases, because Sizzled overexpression markedly stabilized Chordin protein in vivo (compare lanes 2 and 4 in Figure 2D). In contrast, Noggin levels were stable over the 6 hr following injection (Figure 2B, row 2; Sizzled also degraded quite slowly, row 3).

Alternatively, the difference in the long-range patterning ef-fects might be explained by less efficient diffusion of Chordin, which is a much larger molecule than Noggin (Sasai et al., 1994; Smith and Harland, 1992) and thus gives dorsalizing infor-mation over only a short distance. In a fluorescence recovery af-ter photobleaching (FRAP) assay (Sprague and McNally, 2005; Figures S3A–S3H; Movies S1, S2, S3, S4, and S5), the recovery dynamics of monomeric enhanced green fluorescent protein (mEGFP)-tagged proteins (Figure S3B) in the extracellular space were measured after photobleaching within a moderately large area. In this assay, performed under the Sizzled overexpression condition to block Chordin proteinases, mEGFP-Chordin recov-ered quickly from photobleaching (Figures 2E and 2F, blue, and S3F; Movie S3); this quick recovery kinetics was comparable to that of mEGFP (control protein with a signal sequence; Figures

2F, green, and S3E; Movie S1). In contrast, mEGFP-Noggin sig-nals (Figures 2E and 2F, pink, and S3G; Movie S4) recovered only gradually, suggesting that the influx of Noggin from surrounding areas was substantially slower than that of Chordin (Figure 2F). mEGFP-Sizzled exhibited a fast influx tendency (Figures 2E and 2F, purple, and S3H; Movie S5) similar to that of Chordin.

We next performed a fluorescence correlation spectroscopy (FCS) assay in vivo (Chen et al., 2008; Figure S4A). In this assay (Figures S4B and S4D), the EGFP-tagged proteins present in the extracellular space showed distinct diffusion tendencies in faster (D1) and slower (D2) components. Whereas both mEGFP-Chor-din and mEGFP-Noggin exhibited similar ranges of diffusion coefficients in the D1 components (Figure S4C, left column; pre-sumably representing free diffusing populations), their diffusion coefficients in the slower D2 components substantially differed (Figure S4E; 1.9 ± 0.5 and 0.7 ± 0.1 $\mu m^2/\mu s$, respectively, indi-cating that mEGFP-Noggin protein in the D2 component diffused significantly more slowly). Furthermore, the ratio of this slower population was significantly greater for mEGFP-Noggin ($48.0 \pm 4.1\%$) than for mEGFP-Chordin ($22.7 \pm 4.9\%$) (Figure S4F). This substantial presence of the slowly diffusing Noggin popula-tions at the molecular level may be relevant to its strong heparin sulfate binding, which has been reported previously (Paine-Saunders et al., 2002).

Thus, no experimental evidence for slower diffusion of Chordin than Noggin was obtained in either assay, strongly arguing against the second interpretation. Taken together, these obser-vations indicate that Chordin's degradation dynamics are controlled by Sizzled and that this control, rather than its simple diffusion efficacy, is critical for Chordin to properly spread and generate the graded DV pattern in a distance-sensitive fashion (Figure 2G).

Long-Range Chordin-Sizzled Feedback along the DV Axis

To examine the role of endogenous BMP signals in transcrip-tional controls, we next controlled their levels by injecting BMP antagonist (Noggin protein, which is proteinase resistant) into the blastocoel of β-catenin-MO-injected ventralized blastulae (Figures 3A–3C) and measured the transcript levels at stage 13 by quantitative PCR (qPCR). The decrease of endogenous BMP signals by the antagonist efficiently suppressed *sizzled* and *bmp4* expression (Figure 3A), whereas the lateral gene (*myoD*) showed a biphasic response (Figure 3B). In contrast, dor-sal genes (*chordin*, *admp*, *shh*, and *noggin*) were induced in a dosage-dependent manner (Figure 3C; data not shown), showing that different levels of endogenous BMP signaling, without the influence of Wnt signaling, can define at least three distinct phases of response in the *β-cateinin*-MO-injected ventral-default embryo.

In the embryo during the gastrula stages (Figures 3D–3U), expression of *sizzled* was diffuse along the DV axis at the onset of gastrulation (Figure 3D) but soon became limited to the ventral side as gastrulation proceeded (Figures 3E–3G), depending on endogenous Chordin (Figures 3H–3K).

Conversely, *chordin* expression in the dorsal mesoderm (Figures 3L–3O), which is negatively controlled by BMP signals (Inomata et al., 2008), was positively regulated by Sizzled; the
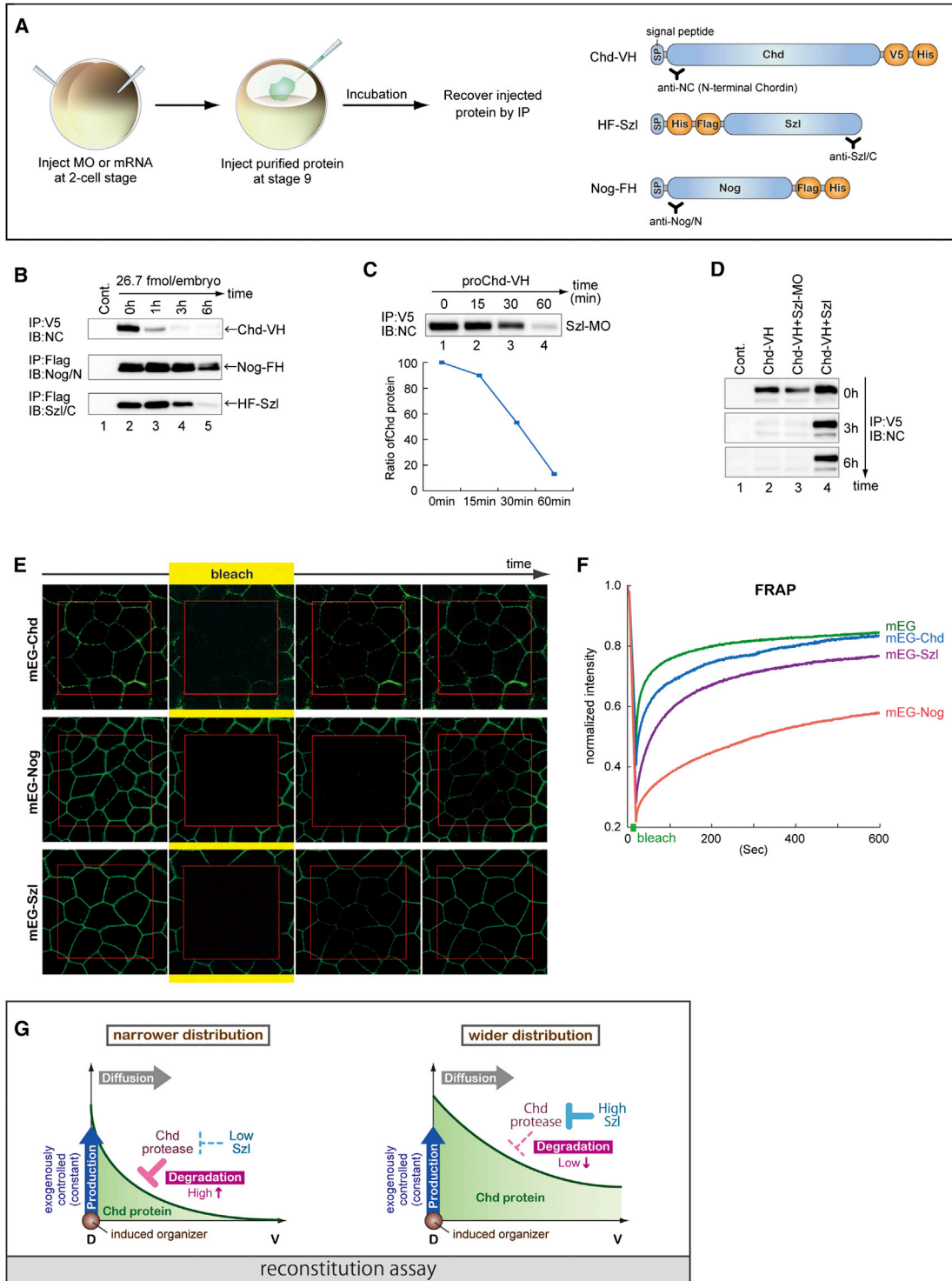
Figure 2. Rapid Proteolysis Limits the Working Range of Fast-Diffusing Chordin

(A) Schematic of blastocoel injection assay. Proteins were immunoprecipitated with a C- or N-terminal antibody and detected with an antibody against the opposite end to selectively measure full-length proteins.

(B and C) Degradation kinetics of recombinant Chordin (B and C), Noggin (B), and Sizzled (B) in the embryo.

(D) Effects of depletion (lane 3) and overexpression (lane 4) of Sizzled on Chordin stability.

(E and F) In (E), FRAP assays of mEGFP-tagged Chordin (top), Noggin (middle), and Sizzled (bottom) shown by snapshots. From left to right columns; before bleaching, at the end of bleaching, 50 s after bleaching, and 230 s after bleaching. (F) Recovery kinetics of mEGFP-tagged proteins. mEG, control (secretable

(legend continued on next page)

inhibition of Sizzled (Figures 3P–3S) substantially reduced *chordin* expression, in particular, during mid- to late gastrulation (Figures 3R and 3S). qPCR experiments also confirmed that *chordin* and *sizzled* each require the other for their expression (Figures 3T and 3U).

Given that Sizzled inhibits Chordin degradation, these findings suggest a feedback loop that dynamically controls *chordin* and *sizzled* expression via Chordin stabilization (Figure 3V; Lee et al., 2006). This feedback system would require long-range interactions because *chordin* and *sizzled* are expressed at opposite ends of the DV axis during mid- to late gastrulation (Figure 3W).

Dynamic Chordin Stability Control by Sizzled Protein Accumulation

We next examined whether the amount of endogenous Sizzled protein is actually influenced by endogenous Chordin, which is produced on the dorsal side. We analyzed endogenous Sizzled protein recovered from the extracellular fluid of the gastrula embryo and found that Chordin depletion led to a marked increase in the amount of Sizzled in vivo (Figure 4A, lane 3, lanes 2 and 4 show the specificity control caused by *sizzled*-MO; see Figure 4B for quantification). In contrast, the accumulation of endogenous Chordin protein, which was particularly obvious at stage 11 and afterward (Figure 4C, top row), decreased substantially when Sizzled was depleted (Figures 4D and 4E). Thus, mutual regulation occurs between endogenous Sizzled and Chordin, even though they are produced in separate domains.

Although total *sizzled* transcription in the whole embryo did not particularly increase during gastrulation (stages 10–13; Figure 3T, black line), the amount of endogenous Sizzled protein gradually increased as gastrulation progressed (Figure 4C, bottom row). This protein accumulation is consistent with the high stability of Sizzled protein shown in the blastocoel injection assay (Figure 2B). With this in mind, we analyzed the degradation of recombinant Chordin protein injected into the blastocoel at stages 9, 10, 11, and 12 (Figures 4F–4J). We found that the level of undigested Chordin protein, measured 1.5 hr after injection, increased as gastrulation progressed (Figures 4G and 4H), demonstrating that Chordin becomes more stable at later gastrula stages in parallel with the accumulation of Sizzled (Figure 4C, bottom). The improved stability of Chordin at stage 11 (Figure 4I, bottom row, lane 2) was reversed by *sizzled*-MO (lane 3). Furthermore, the injection of *chordin*-MO, which strongly increased endogenous Sizzled protein (Figure 4A), enhanced the in vivo stability of recombinant Chordin protein (Figure 4J, bottom, lanes 2 and 3), confirming the presence of the long-range feedback loop illustrated in Figure 3W.

Depletion of BMPs (including ADMP) decreased rather than increased Chordin's stability in the gastrula embryo (Figure 4K, lanes 4 and 5). This phenotype is consistent with the decreased expression of *sizzled*, a BMP target, in the BMP-depleted embryo but appears to go against the assumption of a previous DV patterning model (Ben-Zvi et al., 2008) that Chordin degradation preferentially occurs upon complex formation with BMPs. The stability of Chordin protein (V5-tagged) also decreased in the axis-reconstituted embryo when an additional amount of *chordin* (nontagged) was coinjected (Figure 4L, lanes 3–5; as shown in Figure 1O, this amount of *chordin* injection substantially decreases *sizzled* on the ventral side), mimicking the effect of *sizzled*-MO (lane 8). Reduction of Chordin protein stability was rescued by *sizzled* overexpression (lane 7). Because *dnBMPR* injection did not have strong effects, it is inferred that a long-range influence on *sizzled* expression, rather than just the strength of BMP suppression in the organizer, is important for dynamic Chordin stability.

Taken together, these observations indicate that, in the *Xenopus* embryo, Sizzled mainly mediated control over Chordin's stability, and Sizzled's influence supersedes any potential impact of BMP binding to Chordin. Consistent with this idea, depleting Sizzled caused a dominant DV patterning phenotype over the loss of function of ADMP, a BMP protein implicated in the local negative feedback of Chordin activity (Figures 4M–4P).

"Long-Range Accumulation and Feedback" Model

On the basis of our results, we posit that Chordin and Sizzled form a dynamic feedback loop to control their spatiotemporal distribution at both transcriptional and protein levels (model illustrated in Figure 4Q). In this hypothesis, during early to midgastrulation, the expansion of Chordin's distribution is facilitated by the accumulation of Sizzled, which enhances Chordin's stability (Figure 4Q, middle, red curve). Unlike Chordin, Sizzled is stable and can diffuse over a long distance (Figure 2), becoming widely distributed along the DV axis with a relatively shallow gradient (Figure 4Q, middle, blue curve). As Chordin distribution expands ventrally, it gradually limits the area of *sizzled* expression (indicated by the light green zone), because local BMP signals are reduced in the lateral domain. In turn, this regulation in Sizzled production slows down Chordin's ventral expansion by compromising its stability. As gastrulation continues, the expansion of Chordin distribution by Sizzled and the limitation of the *sizzled*-expressing area by Chordin become largely balanced through this long-range feedback loop, forming a stable, graded DV pattern (Figure 4Q, right).

An important characteristic of this feedback system is that its long-range integration of positional information is mediated by diffusible and stable Sizzled protein, which gradually accumulates over a distance in an axis-wide fashion. Thus, we hereinafter refer to this working hypothesis as the "long-range accumulation and feedback" theory of Sizzled function.

Sizzled-Dependent Reshaping of the DV Pattern after Bisection

To further test this theory, we next examined the dynamics of DV patterning after bisecting the embryo. After physical bisection at the blastula stage, the dorsal half develops into a proportionally

mEGFP) for free-diffusing protein (green). mEG-Chd, tagged Chordin (blue); mEG-Nog, tagged Noggin (pink); and mEG-Szl, tagged Sizzled (purple). Injection was done with 600 pg mRNA.

(G) Schematic of diffusion properties of Chordin.

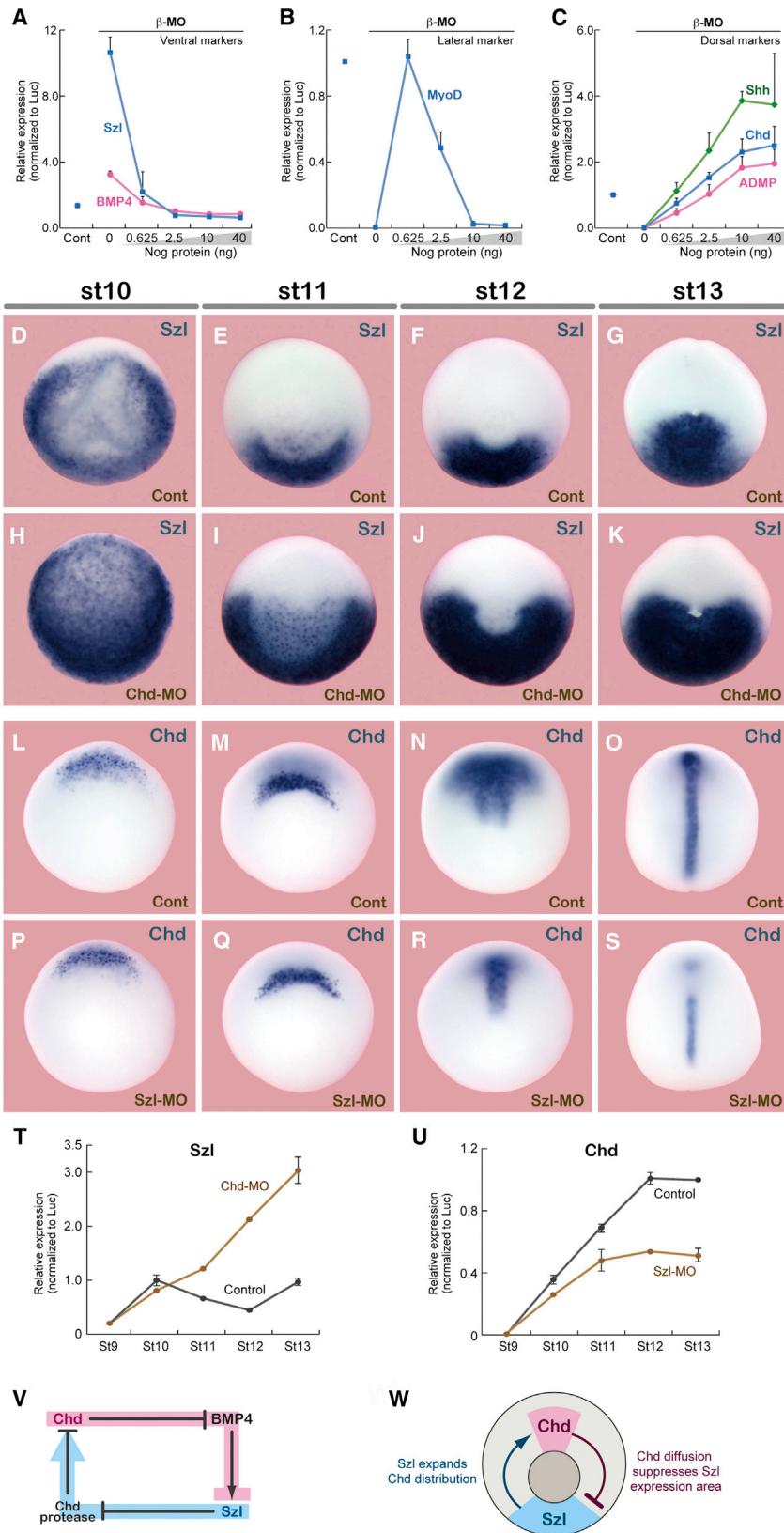See also Figures S3 and S4 and Movies S1, S2, S3, S4, and S5.

A β-MO
Ventral markers

Relative expression (normalized to Luc)

Szl
BMP4

Cont 0 0.625 2.5 10 40
Nog protein (ng)

B β-MO
Lateral marker

Relative expression (normalized to Luc)

MyoD

Cont 0 0.625 2.5 10 40
Nog protein (ng)

C β-MO
Dorsal markers

Relative expression (normalized to Luc)

Shh
Chd
ADMP

Cont 0 0.625 2.5 10 40
Nog protein (ng)

st10   st11   st12   st13

D Szl Cont | **E** Szl Cont | **F** Szl Cont | **G** Szl Cont

H Szl Chd-MO | **I** Szl Chd-MO | **J** Szl Chd-MO | **K** Szl Chd-MO

L Chd Cont | **M** Chd Cont | **N** Chd Cont | **O** Chd Cont

P Chd Szl-MO | **Q** Chd Szl-MO | **R** Chd Szl-MO | **S** Chd Szl-MO

T Szl

Relative expression (normalized to Luc)

Chd-MO
Control

St9 St10 St11 St12 St13

U Chd

Relative expression (normalized to Luc)

Control
Szl-MO

St9 St10 St11 St12 St13

V Chd — BMP4 — Szl — Chd protease

W Chd / Szl
Szl expands Chd distribution
Chd diffusion suppresses Szl expression area

Figure 3. Long-Range Feedback for Expression of *chordin* and *sizzled*

(A–C) qPCR analysis of transcriptional control for *sizzled* and *bmp4* (A, ventral), *myoD* (B, lateral), and *chordin*, *admp*, and *shh* (C, dorsal) in the β-catenin-MO-injected embryo at stage 12 (n = 6; three experiments). The values in qPCR (per embryo) were normalized with the internal control (*luciferase* mRNA) included at the reaction (see Experimental Procedures). The expression levels of the wild-type embryo (Cont; no MO injection) was defined as 1. Increasing amounts of Noggin were injected into the blastocoel of the late blastula as in Figure 2A. Bars represent SD.

(D–K) Expression of *sizzled* in embryos at stages 10 (D and H), 11 (E and I), 12 (F and J), and 13 (G and K). (D) through (G) show control embryos, and (H) through (K) show *chordin*-MO-injected embryos.

(L–S) Expression of *chordin* in embryos at stages 10 (L and P), 11 (M and Q), 12 (N and R), and 13 (O and S). (L) through (O) show control embryos, and (P) through (S) show *sizzled*-MO-injected embryos.

(T and U) Quantification of expression levels of *sizzled* (T) and *chordin* (U) by qPCR (n = 8; three experiments). Bars represent SD.

(V) Schematic of the feedback loop involving Chordin, BMP, Sizzled, and Chordin proteinases.

(W) Simplified view of the axis-wide long-range feedback by Chordin and Sizzled.

patterned embryo along the DV axis, whereas the ventral half forms no axial structures but instead generates a mass of ventral tissues (Figures 5A–5C). To make this remarkable regulatory phenomenon possible, the spatial distribution of DV patterning signals has to be reshaped at the molecular level to compress the morphogen gradient to fit with the shorter body axis (Figure S5A). Indeed, despite this quite destructive perturbation to the system, transcripts of individual dorsal and lateral marker genes (*chordin*, *shh*, *myoD*) in the embryo derived from the dorsal half decreased to about half the levels, in proportion to the smaller expression areas of a half-size body (Figure 5D). The adaptive control in gene expression appeared to occur during gastrulation because the expression levels of *chordin* and *noggin* in the dorsal piece were not reduced at the late blastula stage (stage 9) following the bisection (stage 8) (Figure 5E).

Whole-mount in situ hybridization (Figures 5F–5M; stage 13) also showed that the bisected dorsal piece gave rise to a smaller embryo with dorsal (*shh*+) and ventral (*sizzled*+) tissues reasonably forming at opposite ends (Figures 5F–5I). In the *sizzled*-MO-injected embryo (nonbisected), the expression of the ventral marker expanded dramatically (Figures 5J and 5L). When the Sizzled-depleted embryo was bisected, the expansion of the ventral domain was substantially reduced, in parallel with the removal of the ventral half, whereas the dorsal domain was much the same as it was in the nonbisected *sizzled*-MO-injected embryo (Figures 5K and 5M); thus, scaling failed to occur.

These findings demonstrate an essential role for Sizzled in the long-range feedback for reshaping the DV pattern after development is perturbed by bisection.

A Minimalistic Model of DV Patterning Dynamics

According to our model, bisection may be conceptually considered as a perturbation that substantially removes the Sizzled-producing area (Figure S5B), which may qualitatively contribute to some shrinkage of Chordin's spread by destabilizing it. With this in mind, we next sought to formulate it as a dynamic system of minimal components based on protein interactions, degradation, diffusion, and BMP-regulated production. For simplicity, we considered a one-dimensional mathematical model involving the network of Chordin, Sizzled, Chordin proteinases, BMP4, and ADMP (Figure 6A). In this model, Chordin proteinases degrade Chordin by physical association, whereas Sizzled competitively binds with Chordin proteases. Chordin proteinases, when free from Sizzled, cleave free and BMP-bound forms of Chordin equally. In the latter case, Chordin proteinases release BMPs from Chordin-bound complexes. Local BMP signals (free BMP + ADMP; hereinafter, BMPs) promote the production of BMP4 and Sizzled and suppress that of Chordin and ADMP (Figures 6A and 6B). For positioning the organizer, a basal level of BMP-independent Chordin production is additionally given to the dorsal endpoint. Regarding initial conditions, BMP4 is present evenly at a high level, whereas Chordin, Sizzled, and ADMP proteins are absent at the beginning. The level of Chordin proteinases is assumed to be constant regardless of BMPs signals.

Applying these simple assumptions to the model (see Extended Experimental Procedures for the formulation and parameter settings), we simulated the production and distribution of the proteins. As development proceeded, the production

of Chordin, BMP4, ADMP, and Sizzled proteins along the DV axis converged into stable patterns (Figure 6C, S6A, and S6C), similar to the expression patterns of their transcripts at late gastrulation. Regarding the protein distribution, free BMPs (Figures 6D, red, S6B, and Figure S6D, for each fraction) formed a ventral-high gradient, whereas Chordin was distributed in a reverse gradient (Figures 6D and S6E for BMP-bound fractions only). It is important that, as expected (Figure 4Q), Sizzled protein accumulated widely, on both dorsal and ventral sides (Figures 6E, blue, and S6B), whereas the ventral level was moderately higher.

We next simulated various perturbation-induced phenotypes and compared them with experimental data. First, simulating Sizzled depletion had a strong impact on the DV pattern (Figures 6F and 6G); it predicted the formation of a steeper gradient of BMPs with a larger ventral domain (hyperventralization). In contrast, the depletion of ADMP caused a moderate expansion of the dorsal domain in the simulation (Figure 6H). It is important to note that depleting both Sizzled and ADMP in the simulation predicated a result similar to that of the single Sizzled depletion (Figure 6I). Thus, the depletion of Sizzled had a major influence on DV patterning in the mathematical simulation, as in the real embryo (Figures 4N–4P).

We also introduced substantial changes in the virtual embryo's size, from 500 μm to 1,500 μm (i.e., from the range of bisection to 1.5-fold enlargement), along the DV axis (Figures 6J, 6K, and S6G). Figure 6J shows the calculated distribution of free BMPs, which primarily determine the positional values, along the actual axis length. Importantly, the relative DV patterns deduced from these results (Figure 6K) were largely constant regardless of the changes in size, supporting the system's potential to scale to the axis size.

In the computer simulation of Sizzled depletion, the estimated distribution of free BMPs in the half-size embryo indicated a relative reduction of the ventral domain (Figures 6L and 6M). This simulation result of "imparted scaling" is in good accord with the bisection phenotype of the Sizzled-depleted embryo (Figures 5L and 5M). Notably, the protein distribution of Sizzled changed substantially in response to reductions in embryo size; under the half-size condition, the accumulation level of Sizzled was significantly lower throughout the DV axis, and its gradient became shallower (Figure S6G, blue). This is in sharp contrast to the relative distributions of Chordin (Figure S6G, green) and BMPs (Figure S6G, red), which were largely constant regardless of the size. These findings support the idea that Sizzled plays an active balancing role in the scaling nature of this model.

Collectively, these results from simulation of the minimal model support the logical consistency of the "long-range accumulation and feedback" theory based on Sizzled-mediated feedback.

Embryo Size-Dependent Control of Chordin Degradation via Sizzled

The simulation study suggests that the axis size information is conveyed by the dynamic state of the Sizzled molecule. Finally, to confirm this point experimentally, we examined the embryo-size-dependent control of Chordin's stability, which is a key regulatory event characteristic of this idea. To test the protein stability directly, we again used a reconstitution assay using
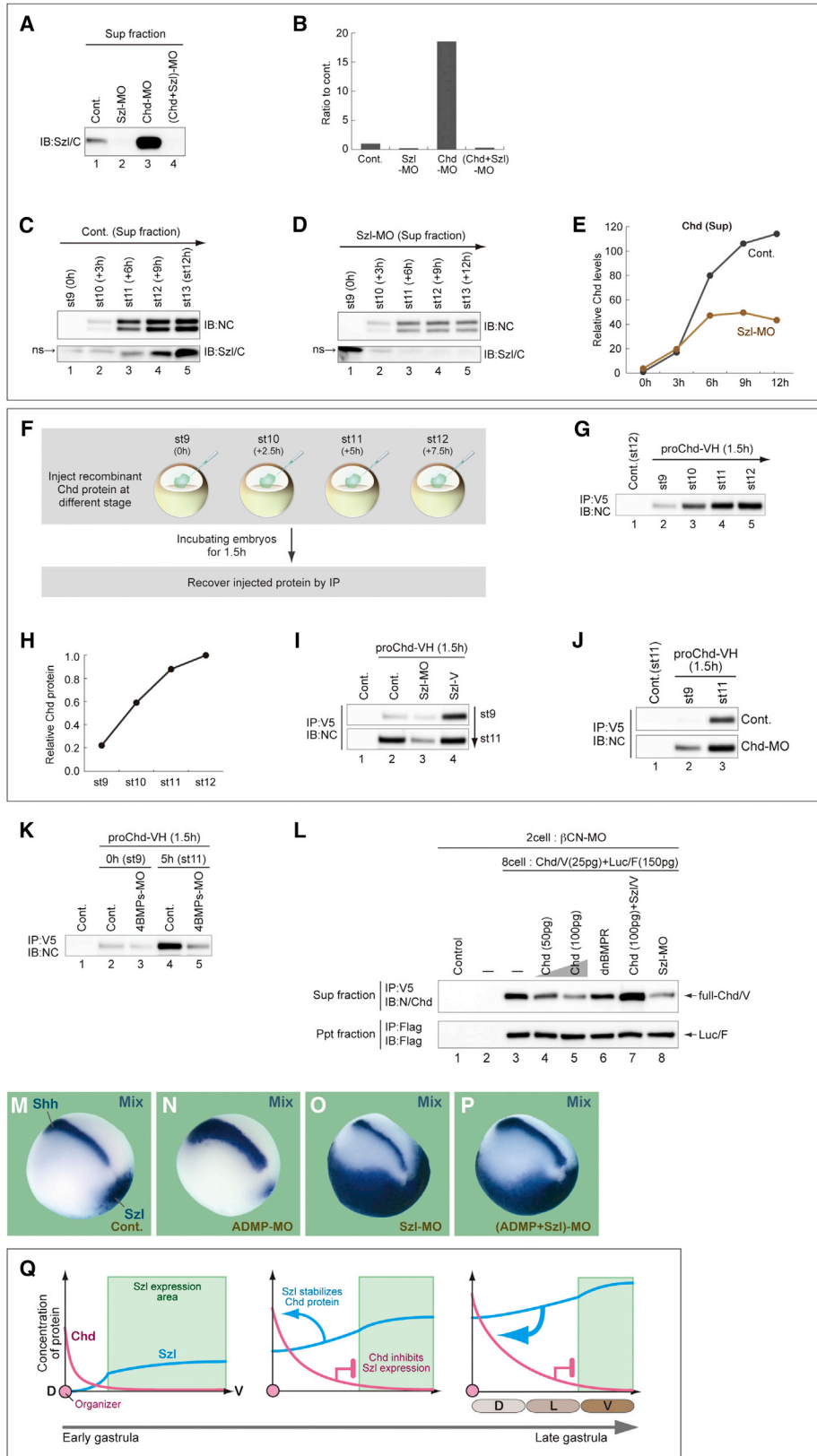
(legend on next page)

β-catenin MO-injected embryos, in which Chordin production can be simply controlled by exogenous mRNA. Axes in the *β-catenin*-depleted embryos were rescued by locally injecting epitope-tagged *chordin* (Figure 7A; injected cells were marked with *mcherry*; Figures S7A–S7D; protein constructs in Figure S7E), which induced a "dorsal" side that carried a constant level of epitope-tagged *chordin*, regardless of the presence or absence of the ventral half. After cellular dissociation at stage 13, supernatant fractions from whole embryos and bisected "dorsal" (mCherry$^+$) and "ventral" (mCherry$^-$) halves were analyzed by western blot (Figures 7B–7D). The amount of epitope-tagged Chordin per embryo was substantially reduced in the bisected "dorsal"-half embryos as compared to that in the same number of whole embryos (Figure 7B, top row, lanes 2 and 3). In contrast, no substantial reduction was seen for a control protein (Figure S7F, top row, lanes 2 and 3). Of note, this difference in Chordin levels was cancelled when Sizzled was depleted (Figure 7C) or overexpressed (Figure 7D), indicating that the Chordin level was reduced by the active regulation of Chordin stability via the feedback loop.

Using the reconstituted embryos, we next examined the extent of Chordin distribution by bisecting them at the early gastrula stage (Figures 7E–7I), instead of the blastula stage. The "injected" and "noninjected" halves were separated and dissociated quickly after bisection to obtain their supernatant fractions. Although a substantial level of epitope-tagged Chordin was detected in the supernatant fraction of the injected halves, little was seen in that of the noninjected halves (Figure 7F, top row, lanes 2 and 3), indicating that Chordin secreted from the injection site had not efficiently reached the other side of the embryo by this stage of development. However, when Sizzled was overexpressed, the noninjected side also contained a substantial level of secreted Chordin (Figure 7G, top row, lane 3). In contrast to Chordin, although the Sizzled (tagged with the NC epitope) was expressed on one side, the other side contained a high level of Sizzled protein (Figure 7H, top row, lane 4). Figure 7I shows the ratio of the protein level in the noninjected halves as compared to the injected halves (also see blot data for control, BMP4, and ADMP proteins in Figures S7G–S7I).

Thus, the effective distribution of Chordin is actively and dynamically controlled by Sizzled, which can itself travel swiftly over the embryonic axis, as expected from the model.

DISCUSSION

Sizzled Accumulation Dynamics Conveys Embryo Size Information

This study demonstrates a crucial role of Sizzled in coupling axis size information with Chordin stability. Our report introduces a real biological example of how spatial information is converted to the state of a regulatory molecule (Figure S7J for further consideration). Unlike previous studies of early *Xenopus* embryogenesis, our present study takes quantitative approaches to estimate three critical parameters for morphogen gradients: production, diffusion and degradation. Based on these analyses, we concluded that the finely modulated degradation dynamics of Chordin by Sizzled, which accumulates in a size-dependent manner, is critical for the DV pattern scaling.

In *Xenopus*, the DV patterning system has multiplex modularity with strong robustness. Our strategy for investigating such a complex dynamic system combined both reductive and constructive approaches. In particular, the in vivo reconstitution assays that we investigated here were very effective for explicitly analyzing critical regulations in the complex system governing the DV patterning.

The Chordin-Sizzled system forms a self-regulatory axis-wide loop that controls Chordin's spatiotemporal distribution. Whereas several other factors have been implicated as feedback regulators in the *Xenopus* DV patterning (e.g., ADMP, Bambi, ONT1, BMP2, and Cv2; De Robertis, 2009; Inomata et al., 2008; Niehrs and Pollet, 1999), this study unambiguously clarified that Sizzled is the essential core regulator of the organizer-dependent scaling system and conveys the information of the embryonic size to which the Chordin gradient is adjusted.

A Dynamic Model for DV Pattern Scaling to Embryo Size

Our model is uniquely based on the differential distribution properties of Chordin and Sizzled. In theory, a diffusible molecule,

---

Figure 4. Dynamically Controlled Protein Accumulation in the Chordin-Sizzled Feedback System

(A–E) Endogenous proteins were recovered from extracellular fluid by dissociating embryos in a small volume of cold CMFM (Ca^{2+}/Mg^{2+}-free medium) with 7.5 mM EDTA at 4°C (5 μl per embryo; 25 μl per lane for loading). In (A) and (B), increase of endogenous Sizzled protein by Chordin depletion (lane 3) is shown by western blot. Sizzled protein in the same number of stage 12 embryos was loaded in each lane. (B) shows protein quantification in (A). The level of Sizzled in the control embryo was defined as 1. (C) through (E) show accumulation of endogenous Chordin and Sizzled proteins during gastrulation. Secreted fractions in the control (C) and sizzled-MO-injected (D) embryos were analyzed. (E) Quantification of protein levels.

(F–H) Stage-dependent Chordin stability was analyzed in the blastocoel injection assay. In (G), the intact form of recombinant Chordin protein was quantified 1.5 hr after blastocoel injection (at stage 9, 10, 11, or 12). (H) shows the line graph presentation of results in (G).

(I) Effects of Sizzled depletion and overexpression on increased stability of recombinant Chordin at stage 11 in the blastocoel injection assay.

(J) Injection of *chordin*-MO (bottom) increased the stability of recombinant Chordin in the blastocoel injection assay.

(K) Depletion of all four BMPs (lane 5) promoted Chordin degradation in the stage 11 embryo.

(L) The amount of intact V5-tagged Chordin protein (top) was decreased when nontagged *chordin* (100 pg; lane 5) was coinjected with V5-tagged *chordin* (25 pg) into a vegetal blastomere of eight-cell embryos (compare with lane 3). *β-CN*-MO, *Sizzled*-MO, and *Szl* mRNA were injected at the two-cell stage. *luc/F* (bottom, injection control) and *dnBMPR* mRNA were injected at the eight-cell stage.

(M–P) Effects of MOs for *admp* and *sizzled* on DV markers. ADMP depletion moderately expanded the expression of the dorsal axial marker and reduced that of the ventral marker; 100%, n = 20, in (N). Sizzled depletion suppressed the dorsal axial marker and dramatically expanded the ventral marker; 100%, n = 14, in (O). Combined depletion of ADMP and Sizzled caused a phenotype similar to that by Sizzled depletion; in (P) 100%, n = 16, for dramatic *sizzled* expansion with no substantial *shh* expansion.

(Q) Schematic of the long-range feedback and accumulation model. Distribution of Chordin and Sizzled along the DV axis is shown in red and blue, respectively. ns, nonspecific band.
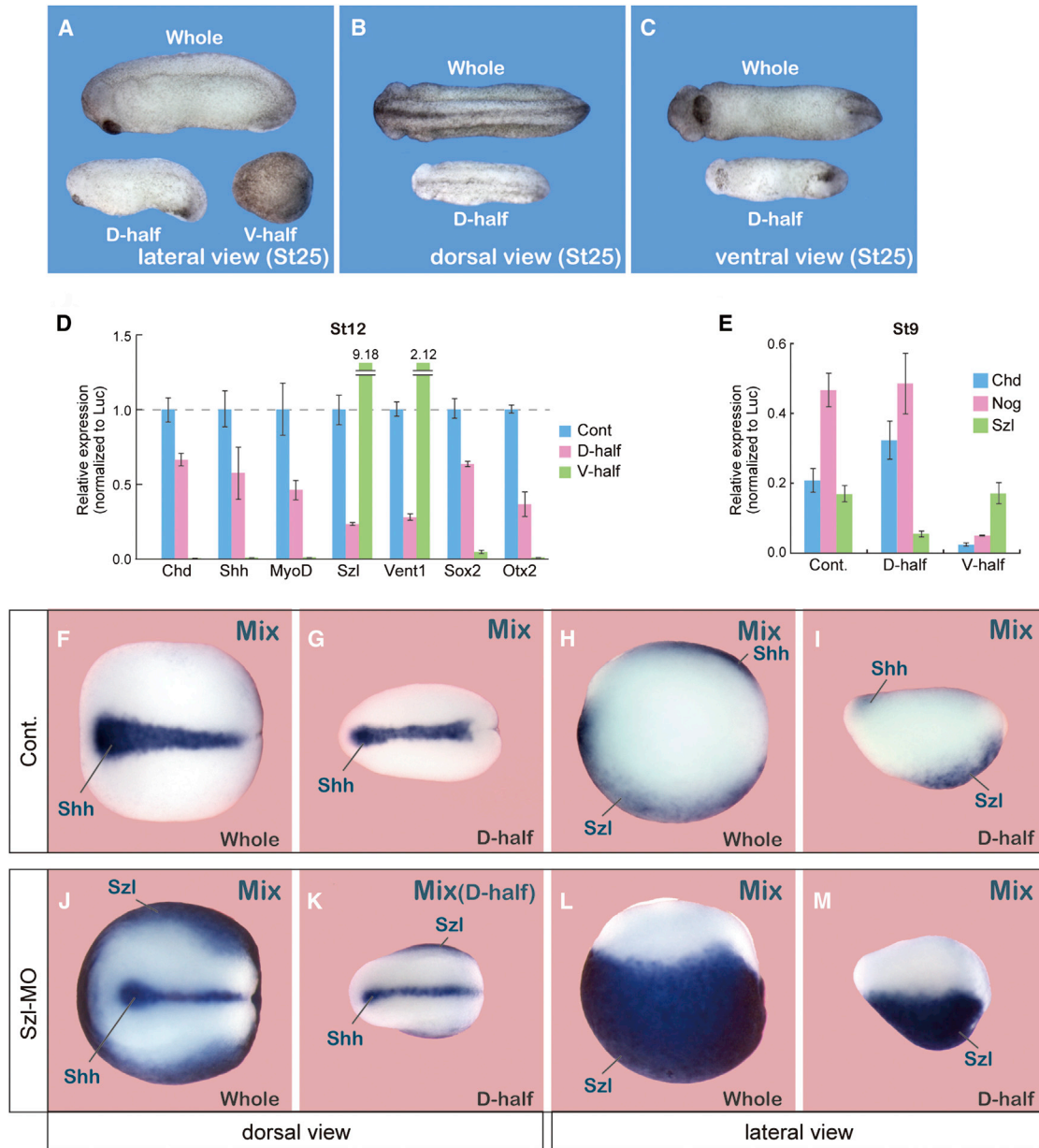
Figure 5. Essential Role of the Chordin-Sizzled System in DV Pattern Scaling after Bisection

(A–C) External phenotypes at the tailbud stage in bisection experiments (bisection was done at stage 8). Lateral, dorsal, and ventral views are shown in (A), (B), and (C), respectively.

(D) Transcript levels of regional markers in the same number of control (blue), dorsal-half (red), and ventral-half (green) embryos (stage 12) shown by qPCR (three experiments). Bars represent SD.

(E) Transcript levels of *chordin* (blue), *noggin* (red), and *sizzled* (green) in the same number of control, dorsal-half, and ventral-half embryos at stage 9 (three experiments). Bars represent SD.

(F–M) Effect of Sizzled depletion on DV marker patterns in bisection conditions. (F) through (I) show uninjected controls. (J) through (M) show *sizzled*-MO-injected embryos. (F), (H), (J), and (L) show whole embryos. (G), (I), (K), and (M) show bisected dorsal halves. (F), (G), (J), and (K) show dorsal views. (H), (I), (L), and (M) show lateral views. (I) Balanced *shh* and *sizzled* expression in 100%, n = 11. (L) shows dramatic *sizzled* expansion in 100%, n = 20. (M) shows disproportionate reduction in *sizzled* expression in 100%, n = 12.

See also Figure S5.

emanating from an origin, spread to form a gradient depending on two parameters: a diffusion coefficient and rate of clearance (e.g., degradation). An important general rule suggested by our study may be that the control of clearance rate can play an active role in operating self-regulatory gradient systems, whereas the diffusion coefficient is molecule specific and difficult to alter in
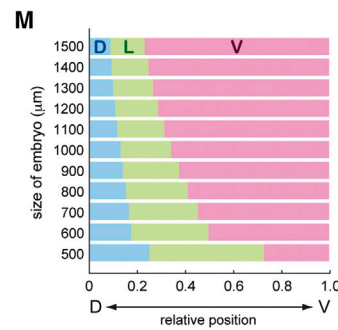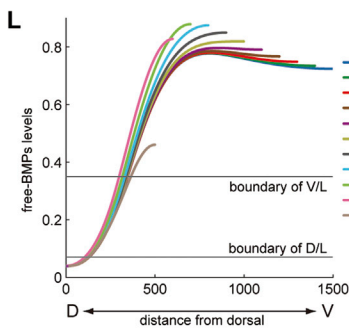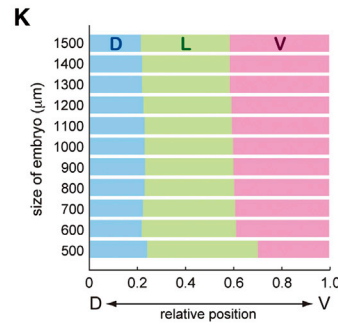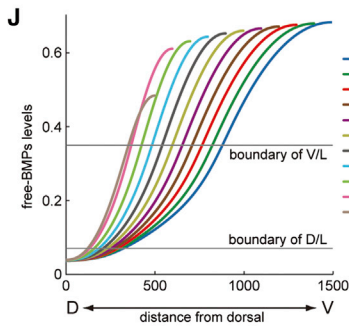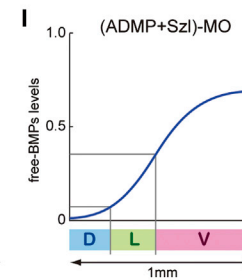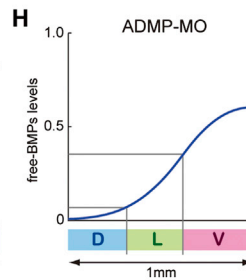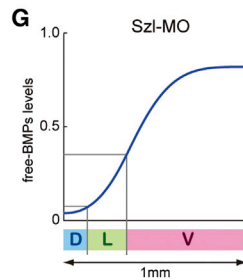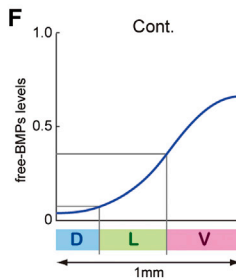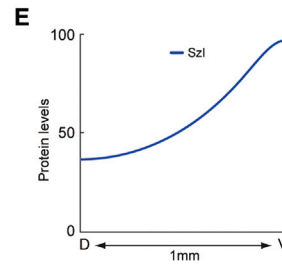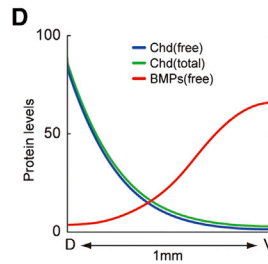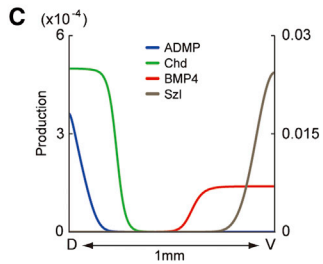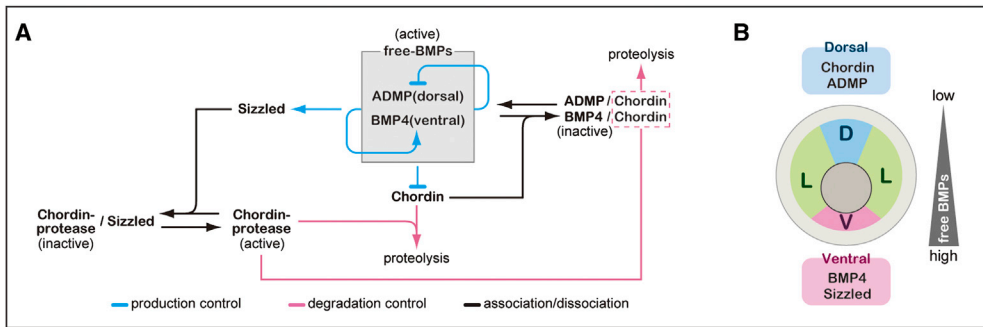
(legend on next page)

a context-dependent fashion. In *Xenopus* DV patterning, Chordin's clearance is dynamically controlled by Sizzled. Sizzled's stability and fast diffusion would form a shallow gradient, allowing the protein to distribute far from the origin—even as far as the opposite side of the embryo as shown in Figure 7. These characteristics appear to give Sizzled an advantage in carrying size-sensitive information from one end of the embryo to the other.

We were also intrigued by the question of how much this system could be reduced in size and still retain scaling ability. Our computer simulations (Figures S6F and S6G) indicated that the average concentration and distribution of Sizzled protein, unlike those of free BMPs, substantially alter with changes in size, suggesting that the dynamic changes of Sizzled distribution plays an active compensatory role (or gives a tradeoff) for lost embryo size. If this idea is correct, a reduction limit of Sizzled should make a bottleneck for the compensation range in pattern scaling. Indeed, the Chordin-Sizzled system cannot contribute indefinitely; an even greater reduction (e.g., to a quarter of the original size) would not allow scaling, leading to hyperdorsalization (Figure S6H), because of insufficient room for adaption by Sizzled (this is in accord with the bottoming out of Sizzled concentrations in Figure S6F). This is in accord with our experimental observation that dorsal blastula tissue, when isolated as a dorsal piece smaller than quarter of the whole embryo, became hyperdorsalized (Figures S6I–S6K). On the other hand, the lack of ADMP, which per se causes a relatively moderate dorsalization (Figures 4N and S6M), still allows the DV pattern to scale but only within a narrower range of size (Figure S6L; this is consistent with the finding that the bisection of ADMP-depleted embryos results in hyperdorsalization; Figures S6M and S6N; Reversade and De Robertis, 2005), suggesting that ADMP is not indispensable for scaling itself but plays a critical role in reinforcing the size-dependent adaptation.

Our simulation showed that the scaling nature of this DV patterning system is consistent at both 20 and 100 hr points (Figures 6K and S6O; it takes about 20 hr for the midblastula *Xenopus* embryo at 16°C to reach the end of gastrulation when the DV fates of tissues becomes fixed; Spemann, 1918). In the embryonic context, the presence of a steady state during the dynamic process of gastrulation may be arguable. For instance, the protein accumulation of Sizzled seemed to increase gradually during late gastrulation (Figure 4C, bottom). Therefore, it could be beneficial that the scaling system proposed in this study is applicable not only to the steady state but also to transient states in the converging process.

Relevance to Other Self-Regulatory Models

Although Sizzled is absent in the *Drosophila* embryo, Sog, Dpp, and Tolloid are implicated in fly DV patterning; a mechanism qualitatively different from the Chordin-Sizzled system has been proposed (Eldar et al., 2002; O'Connor et al., 2006; Shimmi et al., 2005). In this model, Sog-Dpp protein complexes diffuse more efficiently than Dpp alone and are more sensitive to cleavage by Tolloid than Sog alone (Peluso et al., 2011). Computer simulations based on these assumptions (Eldar et al., 2002) have successfully demonstrated a mechanism for the Sog-dependent reinforcement of BMP (Dpp and Scw) signaling in the amnioserosa (Ashe and Levine, 1999), which is located farthest from the Sog-expressing domain, as well as the robustness of the DV pattern against gene dosages in the fly. A similar shuttling mechanism, which does not involve Sizzled, has also been applied to *Xenopus* for modeling DV pattern formation and explaining its adjustment to embryonic size (Ben-Zvi et al., 2008), whereas the requirements (or assumptions) of the model have not been rigorously proven experimentally (Francois et al., 2009). Actually, experimental observations in the present and previous studies do not appear to support the critical requirements (assumptions) of this model (e.g., Figures 4K, S7H, and S7I; also see Extended Experimental Procedures).

There have been a number of previous studies on the mathematical aspect of scaling dynamics (Ben-Zvi et al., 2011; Hecht et al., 2009; McHale et al., 2006; Othmer and Pate, 1980; Umulis, 2009). Self-regulatory systems, which apparently differ in components and contexts, may share particular common mathematical rules in essence. For instance, on a superficial level, our "long-range accumulation and feedback" theory may have some features similar to the expansion-repression model proposed previously as a theoretical framework for scaling (Ben-Zvi and Barkai, 2010). According to the idea, Sizzled, a size-dependent factor, might roughly correspond to an expander of the spread of the morphogen (Chordin) that represses the expander production; however, the presence of common mathematical rules between them needs to be very strictly investigated. Whereas it is certainly beyond the scope of the present molecular embryological study, the mathematical aspects of this information conversion and its consequent regulatory rules are an intriguing future topic for in-depth study in theoretical biology. In conclusion, our experimentation-based study proposes a rigid molecular mechanism for coupling a global gradient field with local signal activity via the axis-wide feedback system.

Figure 6. DV Pattern Scaling in a Minimalistic Model for the Chordin-Sizzled System

(A) Schematic of the molecular interaction network involving minimal components.

(B) Schematic of BMPs-dependent regulation of expression areas.

(C–M) Simulation results at 20 hr. (C) shows regional production of proteins along the DV axis. The production rates are given by the first terms in Equations 1, 2, 3, and 4 shown in the Extended Experimental Procedures. The y axis stands for production levels for ADMP, Chordin, BMP4 (left scale), and Sizzled (right scale). (D) shows simulation results of protein distribution. The y axis stands for protein levels for free Chordin, total Chordin (left scale), and free BMPs (right scale). (E) shows simulated distribution of Sizzled. (F) shows control; (G) through (I) show simulated effects of depletion of (G) Sizzled, (H) ADMP, and (I) Sizzled + ADMP on distribution of free BMPs (top, curve graphs) and DV patterns (bottom, horizontal bar graphs). (J) through (M) show simulated effects of embryo-size reduction on distribution of free BMPs along the actual DV length, in (J) and (L), and on relative DV patterning in (K) and (M); border assignments are the same as in (F) in the control in (J) and (K) and Sizzled-depleted embryos in (L) and (M). In (K) and (M), the horizontal axis indicates relative position along the DV axis with 0 and 1 being most dorsal and most ventral, respectively.

See also Figure S6.
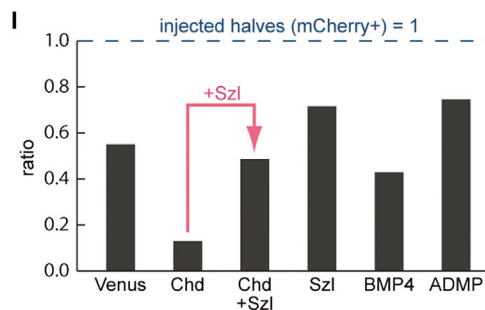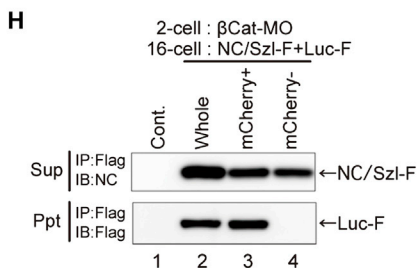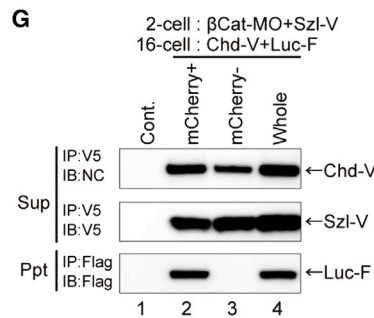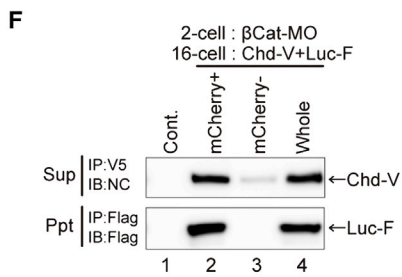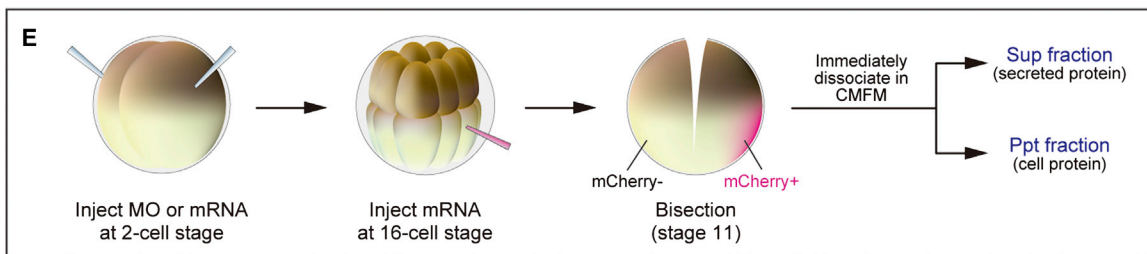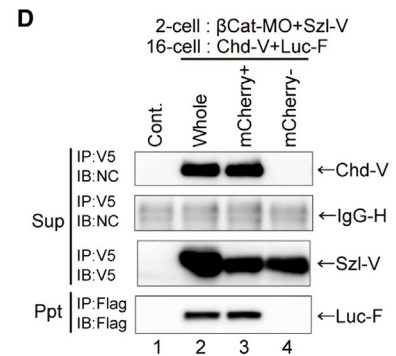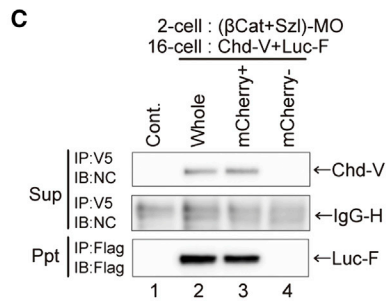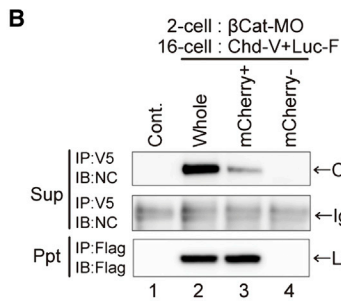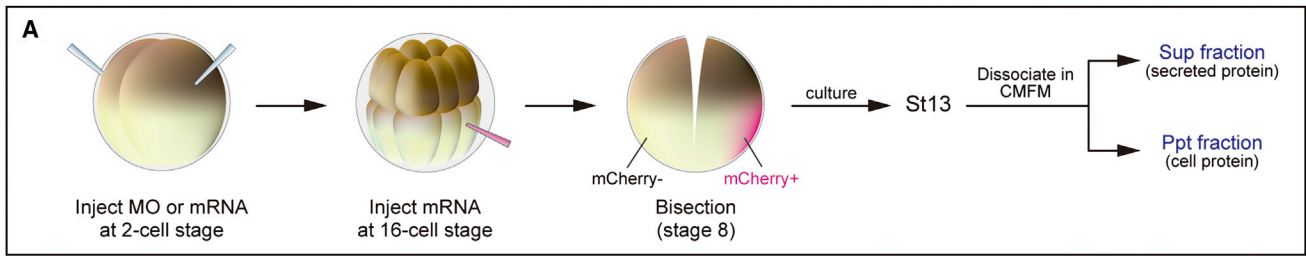
(legend on next page)

EXPERIMENTAL PROCEDURES

Embryonic Manipulation, Protein Assay, and Western Blot

The experimental procedures for embryonic manipulation, RNA injection and whole-mount in situ hybridization were performed as described previously (Sasai et al., 1994; Inomata et al., 2008). We experimentally confirmed that mRNAs for tagged proteins (EGFP, NC, and V5 tags) exert activities comparable to mRNAs for untagged proteins. Detailed information about MOs is available in the Extended Experimental Procedures. For bisection assay, eight-cell embryos with clear polarity in the pigmentation pattern along the DV axis were selected. Then these embryos, when they reached the midblastula stage (stage 8), were cut into dorsal and ventral halves with a Gastromaster micro-dissection device. Bisected pieces were cultured in 0.3× Barth's medium with 0.5% gentamicin (Nacalai Tesque). Blastocoel protein injection, protein assay, and western blot is described in the Extended Experimental Procedures.

FRAP Assay

For FRAP assay, RNA was injected into two animal blastomeres of eight-cell embryos. Their vegetal halves were removed at stage 8, and the remaining portions were cultured until the early gastrula stage. For the flat-mount observations in the FRAP assay, the animal-half tissues were sandwiched between a bottom slide and a coverglass. Detailed information and FCS assay are described in the Extended Experimental Procedures.

In Vivo Reconstitution Assay and Immunostaining

For in vivo reconstitution, β-catenin-MO (8 ng), chordin-MO (16 ng), and noggin-MO (16 ng) were injected into two blastomeres at the two-cell stage. For Sizzled overexpression or depletion, sizzled mRNA (400 pg) or sizzled-MO (8 ng) was also coinjected with other MOs, respectively. At the eight- or 16-cell stage, MO-resistant chordin or noggin mRNA was injected into a vegetal blastomere together with venus mRNA (200 pg), β-gal (200 pg), or mcherry (200 pg) as a tracer. Immunostaining of Xenopus embryos was performed as described elsewhere (Aramaki et al., 2010). Detailed information is available in the Extended Experimental Procedures.

qPCR Assay

The 7500 Fast Real Time PCR System (Applied Biosystems) was used for qPCR assays. To collect mRNAs, embryos were homogenized in buffer RLT (RNeasy Mini Kit; QIAGEN), to which 400 pg luciferase mRNA per embryo was added as internal control. Because standard curves showed a good linearity over the measurement range from 400 ng to 4 pg in qPCR assays (data not shown), the expression level per embryo was thus estimated by normalizing to the luciferase level. Primers used for qPCR are described in the Extended Experimental Procedures.

Mathematical Modeling

Numerical simulations based on mathematical modeling of the "long-range accumulation and feedback" theory were performed as described in Extended Experimental Procedures in detail. Briefly, the time evolution of the concentra-tions of proteins (Chordin, BMP4, ADMP, Sizzled, and Chordin-BMP complexes) is given by the reaction-diffusion equations based on (1) BMP-dependent production, (2) clearance (e.g., Sizzled-controlled proteolysis for Chordin and receptor-mediated internalization for BMPs), (3) formation and dissociation of protein complexes (Chordin-BMPs), and (4) diffusion.

REFERENCES

Aramaki, T., Sasai, N., Yakura, R., and Sasai, Y. (2010). Jiraiya attenuates BMP signaling by interfering with type II BMP receptors in neuroectodermal patterning. Dev. Cell 19, 547–561.

Ashe, H.L., and Levine, M. (1999). Local inhibition and long-range enhancement of Dpp signal transduction by Sog. Nature 398, 427–431.

Ben-Zvi, D., and Barkai, N. (2010). Scaling of morphogen gradients by an expansion-repression integral feedback control. Proc. Natl. Acad. Sci. USA 107, 6924–6929.

Ben-Zvi, D., Shilo, B.Z., Fainsod, A., and Barkai, N. (2008). Scaling of the BMP activation gradient in Xenopus embryos. Nature 453, 1205–1211.

Ben-Zvi, D., Shilo, B.-Z., and Barkai, N. (2011). Scaling of morphogen gradients. Curr. Opin. Genet. Dev. 21, 704–710.

Chen, H., Farkas, E.R., and Webb, W.W. (2008). Chapter 1: In vivo applications of fluorescence correlation spectroscopy. Methods Cell Biol. 89, 3–35.

Christian, J.L., and Moon, R.T. (1993). Interactions between Xwnt-8 and Spemann organizer signaling pathways generate dorsoventral pattern in the embryonic mesoderm of Xenopus. Genes Dev. 7, 13–28.

Cooke, J. (1973). Properties of the primary organization field in the embryo of Xenopus laevis. IV. Pattern formation and regulation following early inhibition of mitosis. J. Embryol. Exp. Morphol. 30, 49–62.

Cooke, J. (1975). Local autonomy of gastrulation movements after dorsal lip removal in two anuran amphibians. J. Embryol. Exp. Morphol. 33, 147–157.

Figure 7. Size-Dependent Control of Chordin Stability

(A) Schematic of reconstitution experiments. The dorsal axis was rescued by a single-blastomere injection of chordin (V5-tagged; 12.5 pg) in the β-catenin-depleted embryo. As a tracer, mcherry (200 pg) was coinjcted for marking the injected site.

(B–D) Effect of bisection on the levels of intact Chordin protein. Lanes 1 show uninjected whole embryos. Lanes 2 show whole embryos with mRNA injection. Lanes 3 show injected halves (mCherry+). Lanes 4 show uninjected halves (mCherry−). IgG-H is the loading control for interexperimental comparison for (B) through (D). In (B), the amount of intact Chordin (top) was decreased in the dorsal halves as compared to that in the same number of the whole embryos. This contrasted the largely constant amounts of control luciferase (bottom; 150 pg luciferase mRNA injection). As shown in (C), when Sizzled was depleted in addition, the amounts of intact Chordin with (lane 3) or without (lane 2) bisection were comparable and low. In the Sizzled-overexpressed conditions in (D), the amounts of intact Chordin with (lane 3) or without (lane 2) bisection were comparable and high.

(E–I) Analysis of long-range protein distribution at the early gastrula stage. (E) Schematic of comparison of protein contents in "injected" (mCherry+) and "un-injected" (mCherry−) halves of the stage 11 embryo. In (F), epitope-tagged Chordin was predominantly detected in the "injected" halves (lane 2). In (G), when Sizzled was overexpressed, epitope-tagged Chordin was detected also in the "uninjected" halves. In (H), Sizzled (12.5 pg), expressed on one side, was detected on the other side. (I) shows ratios of protein levels detected in the "uninjected" halves (the level in the "injected" halves is defined as 1).

See also Figure S7.

De Robertis, E.M. (2009). Spemann's organizer and the self-regulation of embryonic fields. Mech. Dev. *126*, 925–941.

De Robertis, E.M., and Kuroda, H. (2004). Dorsal-ventral patterning and neural induction in Xenopus embryos. Annu. Rev. Cell Dev. Biol. *20*, 285–308.

Eldar, A., Dorfman, R., Weiss, D., Ashe, H., Shilo, B.Z., and Barkai, N. (2002). Robustness of the BMP morphogen gradient in Drosophila embryonic patterning. Nature *419*, 304–308.

Francois, P., Vonica, A., Brivanlou, A.H., and Siggia, E.D. (2009). Scaling of BMP gradients in Xenopus embryos. Nature *461*, E1, discussion E2.

Heasman, J. (2006). Patterning the early Xenopus embryo. Development *133*, 1205–1217.

Hecht, I., Rappel, W.J., and Levine, H. (2009). Determining the scale of the Bicoid morphogen gradient. Proc. Natl. Acad. Sci. USA *106*, 1710–1715.

Inomata, H., Haraguchi, T., and Sasai, Y. (2008). Robust stability of the embryonic axial pattern requires a secreted scaffold for chordin degradation. Cell *134*, 854–865.

Khokha, M.K., Yeh, J., Grammer, T.C., and Harland, R.M. (2005). Depletion of three BMP antagonists from Spemann's organizer leads to a catastrophic loss of dorsal structures. Dev. Cell *8*, 401–411.

Kimelman, D., and Pyati, U.J. (2005). Bmp signaling: turning a half into a whole. Cell *123*, 982–984.

Lee, H.X., Ambrosio, A.L., Reversade, B., and De Robertis, E.M. (2006). Embryonic dorsal-ventral signaling: secreted frizzled-related proteins as inhibitors of tolloid proteinases. Cell *124*, 147–159.

Marom, K., Fainsod, A., and Steinbeisser, H. (1999). Patterning of the mesoderm involves several threshold responses to BMP-4 and Xwnt-8. Mech. Dev. *87*, 33–44.

McHale, P., Rappel, W.J., and Levine, H. (2006). Embryonic pattern scaling achieved by oppositely directed morphogen gradients. Phys. Biol. *3*, 107–120.

Muraoka, O., Shimizu, T., Yabe, T., Nojima, H., Bae, Y.K., Hashimoto, H., and Hibi, M. (2006). Sizzled controls dorso-ventral polarity by repressing cleavage of the Chordin protein. Nat. Cell Biol. *8*, 329–338.

Niehrs, C., and Pollet, N. (1999). Synexpression groups in eukaryotes. Nature *402*, 483–487.

O'Connor, M.B., Umulis, D., Othmer, H.G., and Blair, S.S. (2006). Shaping BMP morphogen gradients in the Drosophila embryo and pupal wing. Development *133*, 183–193.

Othmer, H.G., and Pate, E. (1980). Scale-invariance in reaction-diffusion models of spatial pattern formation. Proc. Natl. Acad. Sci. USA *77*, 4180–4184.

Paine-Saunders, S., Viviano, B.L., Economides, A.N., and Saunders, S. (2002). Heparan sulfate proteoglycans retain Noggin at the cell surface: a potential mechanism for shaping bone morphogenetic protein gradients. J. Biol. Chem. *277*, 2089–2096.

Peluso, C.E., Umulis, D., Kim, Y.J., O'Connor, M.B., and Serpe, M. (2011). Shaping BMP morphogen gradients through enzyme-substrate interactions. Dev. Cell *21*, 375–383.

Piccolo, S., Sasai, Y., Lu, B., and De Robertis, E.M. (1996). Dorsoventral patterning in Xenopus: inhibition of ventral signals by direct binding of chordin to BMP-4. Cell *86*, 589–598.

Piccolo, S., Agius, E., Lu, B., Goodman, S., Dale, L., and De Robertis, E.M. (1997). Cleavage of Chordin by Xolloid metalloprotease suggests a role for proteolytic processing in the regulation of Spemann organizer activity. Cell *91*, 407–416.

Reversade, B., and De Robertis, E.M. (2005). Regulation of ADMP and BMP2/4/7 at opposite embryonic poles generates a self-regulating morphogenetic field. Cell *123*, 1147–1160.

Reversade, B., Kuroda, H., Lee, H., Mays, A., and De Robertis, E.M. (2005). Depletion of Bmp2, Bmp4, Bmp7 and Spemann organizer signals induces massive brain formation in Xenopus embryos. Development *132*, 3381–3392.

Sasai, Y., Lu, B., Steinbeisser, H., Geissert, D., Gont, L.K., and De Robertis, E.M. (1994). Xenopus chordin: a novel dorsalizing factor activated by organizer-specific homeobox genes. Cell *79*, 779–790.

Shimmi, O., Umulis, D., Othmer, H., and O'Connor, M.B. (2005). Facilitated transport of a Dpp/Scw heterodimer by Sog/Tsg leads to robust patterning of the Drosophila blastoderm embryo. Cell *120*, 873–886.

Smith, W.C., and Harland, R.M. (1992). Expression cloning of noggin, a new dorsalizing factor localized to the Spemann organizer in Xenopus embryos. Cell *70*, 829–840.

Spemann, H. (1918). Über die Determination der ersten Organanlagen des Amphibienembryo [On the determination of the first organ anlagen of the amphibian embryo]. Wilhelm Roux Arch. Entw.-Mech. Org. *43*, 448–555.

Spemann, H., and Mangold, H. (1924). Über induktion von Embryonalagen durch Implantation Artfremder Organisatoren [On induction of embryonic anlagen through implantation of foreign organizers]. Wilhelm Roux Arch. Entw.-Mech. Org. *100*, 599–638.

Sprague, B.L., and McNally, J.G. (2005). FRAP analysis of binding: proper and fitting. Trends Cell Biol. *15*, 84–91.

Umulis, D.M. (2009). Analysis of dynamic morphogen scale invariance. J. R. Soc. Interface *6*, 1179–1191.